

Event-driven Video Frame Synthesis

Zihao W. Wang, Weixin Jiang, Aggelos Katsaggelos, Oliver Cossairt
Computer Science & Engineering, Northwestern University
{winswang, weixinjiang2022}@u.northwestern.edu

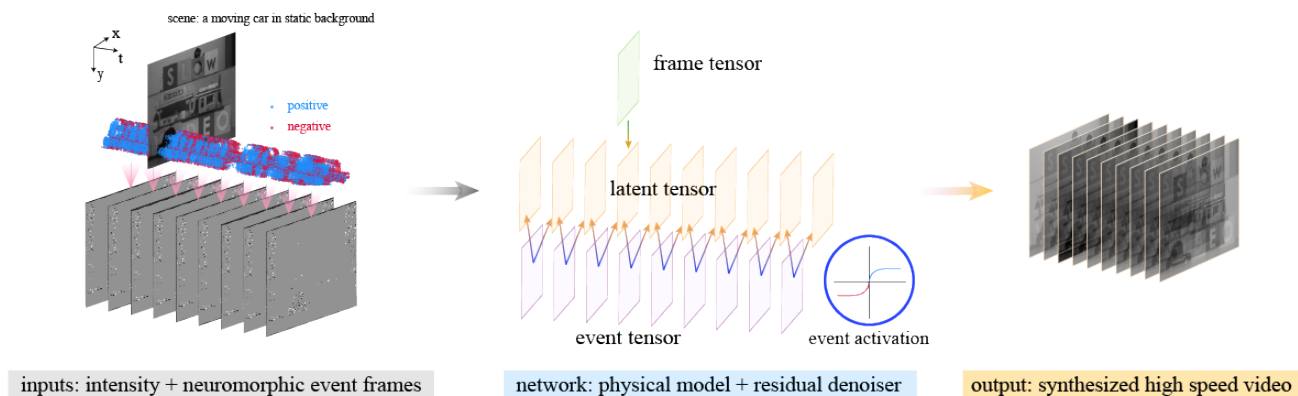


Figure 1: Given two streams of inputs, *i.e.*, reference video frame(s) and neuromorphic events (left), our neural network style optimization framework (middle) approximates the observations as two lower dimensional projections from a latent variable tensor. Specifically, the binary events serve as fixed connecting "weights" and the event sensing process is approximated by tanh activation units. The "training" process minimizes of the losses of the two streams as well as priors. After the optimization, the variable tensor output is a synthesized high frame-rate video.

Abstract

Video frame synthesis is an active computer vision problem which has applications in video compression, streaming, editing, and understanding. In this work, we present a computational high speed video synthesis framework. Our framework takes as inputs two types of data streams: an intensity frame stream and a neuromorphic event stream, which consists of asynchronous bipolar "events" which encode brightness variations over time at over 1000 fps. We introduce an algorithm to recover a space-time video from these two modes of observations. We factor the reconstruction into a physical model-based reconstruction (PBR) process and a residual denoising process. We use a differentiable model to approximate the physical sensing process, which enables stochastic gradient descent optimization using automatic differentiation. Residual errors in PBR reconstruction are further reduced by training a residual denoiser to remove reconstruction artifacts. The video output from our reconstruction algorithm has both high frame rate and well-recovered spatial features. Our framework is capable of handling challenging scenes that include fast mo-

tion and strong occlusions.

1. Introduction

Video cameras capture video signals at a fixed time rate and output signals in a frame-by-frame manner. Under this circumstance, when the motion in the scene is significantly faster than the capturing speed, motion is usually under-sampled and captured videos result in motion blur or large discrepancies between consecutive frames. A direct solution is to use high-speed cameras for fast-varying scenes, but this usually comes with increased hardware complexity, degraded spatial resolution and/or reduced signal-to-noise ratio. On the other hand, high frame rate cameras capture redundant information in adjacent video frames when scene motion is slow.

High speed motion can be acquired more efficiently by employing "event" pixels. Event sensors, or Dynamic Vision Sensors [24, 7], are a breed of bioinspired neuromorphic vision sensors. Each DVS pixel independently detects logarithmic temporal intensity changes and outputs bipolar address-events. This new sensing modality has salient ad-

vantages over frame-based cameras: 1) the asynchronism of event pixels results in an equivalent temporal resolution that is sub-millisecond; 2) since each pixel responds only to intensity changes, the temporal redundancy and power consumption can be significantly reduced; 3) sensing intensity in logarithmic scale enlarges dynamic range to over 120 dB. However, the bipolar output limits spatial contrast and exaggerates noise.

In this paper, we propose a framework for high speed video frame synthesis by combining motion information in the form of both low speed intensity-based and high speed event-based camera measurements. As shown in Fig. , our approach first converts events to frames (left panel). The event frames serve as "bridges" connecting consecutive synthesized intensity frames. We construct an end-to-end, differentiable network to perform physically model-based reconstruction (PBR) (middle panel). Residual errors in PBR reconstruction are further reduced by training a CNN-based residual denoiser to remove reconstruction artifacts. Our results show that our learned denoiser can suppress PBR-introduced "noise" more effectively than a general denoiser.

Our main contributions are summarized as follows:

- We introduce a framework for video frame synthesis based on both intensity frame and event stream input¹. We demonstrate that event information can be used to recover video frames with improved accuracy relative to using intensity information alone.
- We introduce a differentiable physical model that can be optimized using automatic differentiation within a deep learning framework (TensorFlow). We use our model to demonstrate that event information can effectively be incorporated to 1) predict one or multiple frames from current frame; 2) interpolate multiple frames between two frames; 3) recover a motion video from a single blurry frame, *etc.*
- We introduce a residual "denoiser" to learn the reconstruction behavior from the physical model and overcome the artifacts from PBR.

Admittedly, one major limitation of our framework is that it requires processing events in "frame" form. Ideally, one-event-per-frame would preserve the most motion information for our model. However, this would also result in unfeasibly large data volumes. As a compromise, we reduce the temporal resolution of events by binning them together in time using a union operation. This has the effect of simultaneously reducing the temporal resolution of events, as well as the data size of recovered videos. This results in a smaller event stream that is at once 1) compatible with

¹Example codes can be found at <https://github.com/winswang/int-event-fusion>

our physical model, 2) tractable for learning with our CNN-denoiser, and 3) tractable for reconstructing with our PBR and CNN-denoiser.

2. Related work

Here, we briefly review previous work in computational high speed video cameras, applications of event cameras, and video frame synthesis.

Computational high speed cameras. High speed cameras have applications in sports/activity recording and broadcasting, biophysical process detection and analysis, and aerospace exploration. While some consumer grade high speed cameras exist, it remains a significant challenge to simultaneously capture high temporal resolution (TR) and high spatial resolution (SR) videos. To bridge the gap between still cameras (high SR, low TR) and video cameras (low SR, high TR), several methods [8, 40, 15] have been proposed that utilize inter-frame correspondences via optical flow and/or space-time regularization [39, 41]. In addition, methods have been proposed for flexible [16], adaptive [47], and compressive [42] sampling and reconstruction [21] of high speed videos. Gupta *et al.* [16] proposed multi-level SR-TR sampling and post-processing schemes enabled motion-aware videography. Tarvainen *et al.* [43] leveraged spatial-temporal information as camera parameters for super resolution. A number of compressive video sensing [2], prototypes [37, 26] have been devised with additional spatial-temporal encoders and compressive sensing algorithms for data recovery and inference. A recent work demonstrated single-shot 3D video recovery by incorporating active illumination [45].

Vision applications of event cameras. Compared to conventional frame based cameras, event cameras have several advantages, *e.g.*, high temporal resolution, wide dynamic range and low power consumption. The fast response rate can be used for high speed motion tracking and pose estimation [22, 36]. The unique sensing mechanism of event pixels, which respond only to brightness variations, enables inexpensive detection and computation of motion flow [5, 11, 38]. In particular, Benosman *et al.* [5] have demonstrated a simple flow estimation approach by fitting a local plane to a cluster of events. The output form of event cameras, *i.e.*, asynchronous bipolar streams, can effectively encode spatio-temporal relationships and has made event cameras useful for 3D reconstruction [30, 35] and feature detection [31, 4]. Recent advances driven by deep learning has enabled novel applications, such as vehicle steering prediction [29].

Many of the aforementioned applications involve a pre-processing step to convert the event streams to a frame-based format. Recent research efforts have investigated recovering improved intensity images from events [13, 4, 3,

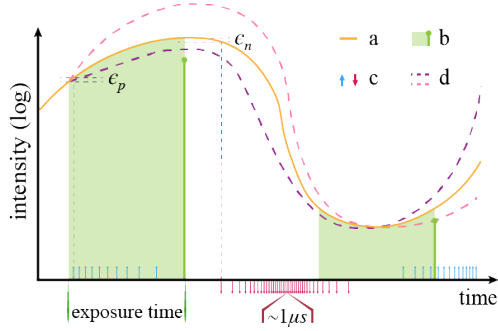


Figure 2: A per-pixel view of the two sensing modes. Given a continuous time-varying signal (a), a camera pixel outputs intensity values (b) with large time intervals due to fixed/low frame rate; an event pixel outputs asynchronous bipolar events (c) which provide “thresholded” gradient information over time. However, “event-guided” interpolation/extrapolation may still have a large solution set due to the ambiguity of *binary* events.

33]. In [13], Cook *et al.* designed a network to interpret events by recurrently interconnected areas, each of which encodes a different aspect of the visual interpretation, such as light intensity or optical flow. Later improvements for intensity reconstruction include patch-based sparse dictionary [4], spatial-temporal regularization via ADMM [3] and manifold regularization [33].

Video frame synthesis. Video frame synthesis is a classic computer vision topic and has applications in video compression, frame rate conversion, motion field estimation, and video editing/rendering. Early work on video frame interpolation and extrapolation focused on establishing block-wise [1, 12] and/or pixel-wise [23, 28] correspondences between available frames. In particular, pixel-wise optical flow methods are commonly used, which assume local brightness constancy [18, 27]. Implementation schemes for improved performances include coarse-to-fine estimation [6], texture decomposition [46], and deep networks [20]. Recent work has focused on constructing end-to-end deep neural networks to bypass optical flow estimation. In [25], a voxel flow layer was inserted in a convolutional neural network (CNN). Niklaus *et al.* [34] forms frame interpolation as a local convolution process and trained a CNN with gradient loss and color loss. Novel architectures, *e.g.*, Generative Adversarial Networks (GAN) [9], and loss functions, *e.g.*, transitive consistency loss [19], have also been proposed for multi-scale frame interpolation and extrapolation.

3. Our fusion algorithm

We pose the problem of frame interpolation as a data inference (interpolation/extrapolation) problem. Figure 2 shows a per-pixel view of our image sensing model. Assume the orange curve (a) is a continuous time-varying signal. The intensity pixel (b) samples the signal at a low and fixed frame rate, with a certain integration time. Meanwhile, the event pixel responds to intensity changes in log scale with very low time latency ($\sim 1\mu s$). That is, as long as the log-intensity increases above a threshold ϵ_p or decreases below a threshold ϵ_n , the pixel will report a binary signal (positive or negative). The event pixels preserve differential information, but the absolute gradient of the intensity is lost. Thus, the data inference problem is ill-posed and results in many solutions, such as (d). This problem can be alleviated by performing optimization over a space-time volume with spatio-temporal regularizers. We propose a differentiable forward model to approximate the physical sensing process of event sensors. We further propose a residual learning scheme to correct for artifacts in the physical model-based reconstruction.

3.1. Physical model

Assume there exists a high frame-rate space-time volume denoted by tensor $\mathcal{H} \in \mathbb{R}^{h \times w \times d}$. In our case, $d > 1$. We seek to recover this signal from two streams of lower-order observations as inputs, *i.e.*, intensity frame(s) and neuro-morphic events.

Intensity observation. We denote the intensity frame observation as,

$$\mathcal{F} = \mathcal{A}(\mathcal{H}), \quad (1)$$

where \mathcal{A} is the intensity sensing operator and \mathcal{F} is the observed intensity frame tensor. For example, if the frame observation has short exposures but large strides of N , the frame tensor can be constructed as slices along the time axis of the latent tensor, *i.e.*, $\mathcal{F}_t = \mathcal{H}_{Nt+N_0}$, where \mathcal{F}_t denotes the frame at time t and similarly, \mathcal{H}_t denotes the latent tensor at time t , $t = 0, 1, 2, \dots$. If the frame observation has a large exposure which spans $S < N$ slices of the latent tensor, the image frame observations can be expressed as $\mathcal{F}_t = \sum_{s=0}^S \mathcal{H}_{Nt+N_0+s}$.

Event activation. We denote the event generation process as an operation \mathcal{B} from the high resolution (high-res) tensor \mathcal{H} ,

$$\mathcal{E} = \mathcal{B}(\mathcal{H}), \quad (2)$$

where \mathcal{E} represents the event frame(s). As mentioned before, an event is fired when the log-intensity of a certain pixel varies beyond a threshold. An example of the observations is shown in Row 1 of Fig. 3. Frame 1 and 2 are two

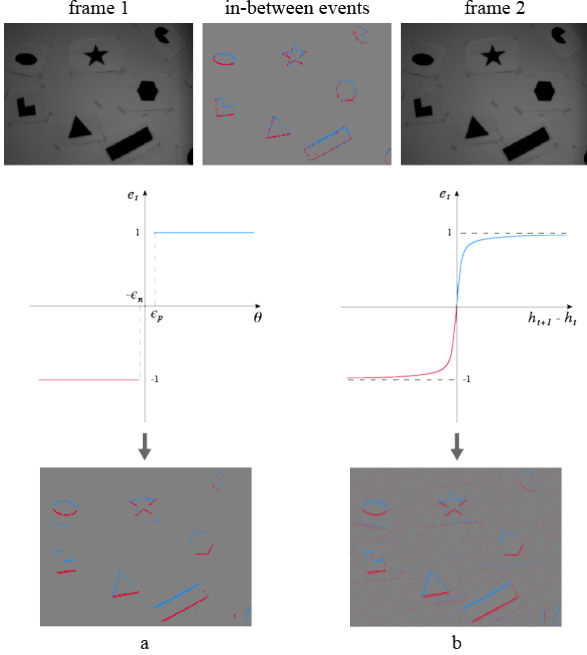


Figure 3: Row 1: two consecutive intensity frames and the events fired in-between. (a) the event firing process; (b) our proposed differentiable model of the event firing process. h_t denotes a pixel of \mathcal{H}_t .

consecutive intensity frames captured at video frame-rate. The events fired between the two frames are shown in the middle column. The event firing process can be mathematically expressed as,

$$e_t = \begin{cases} 1 & \theta > \epsilon_p \\ -1 & \theta < -\epsilon_n \\ 0 & \text{otherwise} \end{cases}, \quad (3)$$

where $\theta = \log(I_t + b) - \log(I_0 + b)$. Note that $e_t = 0$ indicates that the event pixel does not fire. This property reduces data redundancy if there is no motion in the scene. However, Eq. (3) is non-differentiable. In order to approximate this event firing process, we model each event frame as a function of the current and next time slices of \mathcal{H} , *i.e.*,

$$\mathcal{E}_t = \tanh \left\{ \alpha [\mathcal{H}_{t+1} - \mathcal{H}_t] \right\}, \quad (4)$$

where α is a tuning parameter adjusting the smoothness of the activation curve. A comparison of the two activation functions can be viewed in Row 2 and 3 of Fig. 3.

3.2. Physical model-based reconstruction (PBR)

Our physical model-based reconstruction is performed by minimizing a weighted combination of loss functions, including the pixel loss (\mathcal{L}_{pix}) and the sparsity loss (\mathcal{L}_{TV}). The objective function can be formed as,

$$\hat{\mathcal{H}} = \underset{\mathcal{H}}{\operatorname{argmin}} \mathcal{L}_{pix}(\mathcal{H}, \mathcal{F}, \mathcal{E}) + \mathcal{L}_{TV}(\mathcal{H}) \quad (5)$$

Pixel loss. The pixel loss includes per-pixel difference loss in ℓ_1 form with respect to the intensity and event pixels, *i.e.*,

$$\mathcal{L}_{pix}(\mathcal{H}, \mathcal{F}, \mathcal{E}) = \mathbb{E}_{f_{pix}} [\|\mathcal{F} - \mathcal{A}(\mathcal{H})\|_1] + \lambda_e \mathbb{E}_{e_{pix}} [\|\mathcal{E} - \mathcal{B}(\mathcal{H})\|_1], \quad (6)$$

over the entire available data range. \mathcal{F} and \mathcal{E} denote respectively the ground truth of the frame and event data, and \mathbb{E}_x represents expectation with respect to the observed pixels/events.

Sparsity loss. We employ total variation (TV) sparsity in the spatial and temporal dimensions of the high-res tensor \mathcal{H} . The TV sparsity loss is defined as:

$$\mathcal{L}_{TV}(\mathcal{H}) = \lambda_{xy} \mathbb{E}_{h_{pix}} [\|\mathcal{H}_{xy}\|_1] + \lambda_t \mathbb{E}_{h_{pix}} [\|\dot{\mathcal{H}}\|_1], \quad (7)$$

where $\mathcal{H}_{xy} = \frac{\partial \mathcal{H}}{\partial x} + \frac{\partial \mathcal{H}}{\partial y}$ and $\dot{\mathcal{H}} = \frac{\partial \mathcal{H}}{\partial t}$.

By forming the problem into a differentiable physical model, one is enabled to recover the latent high-res tensors using gradient descent based methods in large scale. We optimize Eq. (5) using stochastic gradient descent with TensorFlow implementation. More details are described in Section 4.

3.3. Binning event frames

Here, we analyze the effect of time binning on our physically-based reconstruction. We perform future frame prediction given one current frame and binned event frames with different time windows. The results are summarized in Fig. 4. The top row shows that using a large time window to bin into a single event frame results in clustered event areas located mostly around the edges in the scene. As we decrease the time window to bin events, producing instead 5 binned event frames, each event frame contains fewer events and presents clearer object edges. The resulting reconstruction performance improves as well. However, the trend does not continue as we further increase the binning frame number. When we reduced the time window further to produce 20 binned event frames, very sparse events can be seen in each frame and the resulting reconstruction performance does not improve, since the shown reconstructed frame is closer to frame 1 instead of frame 2. This experiment indicates that the reconstruction performance is closely related to the structure of the binned event frames. Empirically, we observe that the reconstruction performs better when the binned event frames contain clear structure of the scene edges.

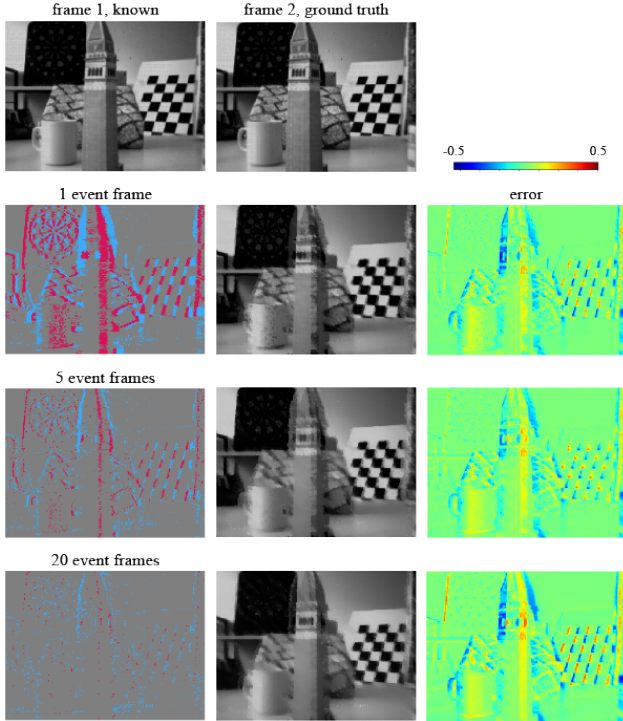


Figure 4: Binning event frames with different time windows. Row 1: ground truth intensity frames. Row 2: left, binning into 1 event frame; middle, reconstructed frame 2; right, error map. Row 3: binning into 5 event frames. Each event frame contains less events. Shown is the last (5th) event frame. Row 4: binning into 20 event frames. Each event frame contains sporadic events. Shown is the 20th event frame.

3.4. Learning a residual denoiser

In order to further improve the frame synthesis results, we treat the artifacts after the PBR as "noise" and perform a "denoising" process. Inspired by ResNet [17] and DnCNN [48], we employ the residual learning scheme and train a deep neural network for denoising the PBR images. As shown in Fig. 5, our network is trained based on the PBR results. That is, we employ the CNN to find the residual \mathcal{R} such that,

$$\mathcal{R} = \hat{\mathcal{H}} - \mathcal{H}_g, \quad (8)$$

where $\hat{\mathcal{H}}$ denotes the reconstructed frame, \mathcal{H}_g denotes the ground truth frame. Note that the reconstructed frame at each epoch and the corresponding residual serve as a training pair. We use a random augmentation scheme, detailed in Section 4, to incorporate a range of PBR results in order to learn a generalized residual network.

Our residual denoiser has two properties. First, the residual denoiser is tightly coupled with the physical model as

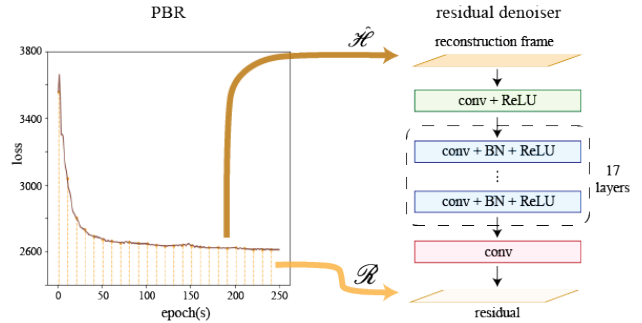


Figure 5: Residual learning. We propose to train a residual denoiser coupled with our PBR process. PBR frames are used as the network input. The residual between the PBR frame and the ground truth frame is the output.

all the training samples are produced via randomized PBR processes. This tight coupling enables the learned residual denoiser to perform better than a general denoiser. Second, our residual denoiser is used after PBR, which preserves the properties of PBR. The benefit of training a CNN to remove artifacts from the PBR is that it can be used recursively to synthesize multiple successive video frames.

4. Implementation details

4.1. Datasets.

In our experiments, we focus on two datasets: the Need for Speed dataset [14] and the event-camera dataset [32]. We use the Need for Speed dataset [14] for training our residual denoiser. The reason we choose this dataset is because it has rich motion categories and content which involves both camera and scene/object motion. The dataset consists of 100 videos (380K frames) captured with now commonly available higher frame rate (240 FPS) cameras from real world scenarios.

4.2. Sample preparation.

The training samples for our residual denoiser are generated by feeding simulated intensity and events through the PBR process. We use our physical model to solve a single-frame prediction problem, as shown in Fig. 6. Given two consecutive video frames, we first simulate the latent event frame. We then perform frame prediction using one of the intensity frames and the simulated event frame. We randomly split the dataset into 89 training classes and 11 testing classes. Only the 240 FPS video frames in the dataset are used for training. To augment the training set, we perform a random temporal flip and a spatial crop with size 40×40 . During preparation of the training samples, the parameters are randomized for the event simulation and frame prediction processes. This is because different parameter

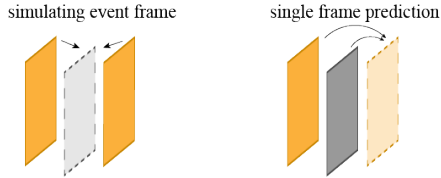


Figure 6: Preparing training samples for residual learning. Left: the event frame simulation described in Eq. (3). Right: single frame prediction using PBR.

source	notation	value range
Eq. (3)	ϵ_p, ϵ_n	(0, 0.05)
Eq. (4)	α	(8, 20)
Eq. (6)	λ_e	(0.1, 0.5)
Eq. (7)	λ_{xy}	(0.3, 0.8)
Eq. (7)	λ_t	(0.2, 0.6)
	event percentage	(0%, 20%)
	PBR learning rate	(0.0065, 0.009)
	PBR epoch(s)	(1, 250)

Table 1: Augmentation recipe

combinations can result in widely varying reconstruction performance. Randomizing these parameters forces our learning algorithm to generalize to a wide range of scene, reconstruction and imaging conditions. A summary of our augmentation recipe is presented in Table. 1. Note that we enforce generated event frames to contain less than 20% of events.

4.3. PBR

In our physical model-based reconstruction process, we initialize the high-res tensor \mathcal{H} by nearest neighbor interpolation of low resolution observed intensity frames \mathcal{F} . The observed event frames input to the algorithm have only three values, $\{-1, 0, 1\}$. Our algorithm is implemented in TensorFlow. On average, the run time for processing (CPU) a single frame prediction with size 180×240 is 0.0268 second per epoch.

4.4. Training and testing.

We generate 100K image pairs of size 40×40 pixels; 80% of the sample dataset are randomly chosen as training samples and the rest 20% are used for validation. We use a batch size of 128, which results in 2K batches per epoch. We use mini-batch stochastic gradient descent with an Adam optimizer ($\beta_1 = 0.9, \beta_2 = 0.999$). The learning rate is scheduled as 1×10^{-3} for the initial 30 epochs, then 1×10^{-4} for the following 30 epochs and 5×10^{-5} afterwards. We use an NVIDIA TITAN X GPU for parallelization. Each epoch takes approximately 6 minutes training on

our machine. We train our network for 150 epochs.

Since our model is fully convolutional, the number of parameters is independent of the image size. This enables us to train on small patches (40×40) and test on the whole image. For an image of size 180×240 , the testing time is 0.02 second on average.

5. Results

In this section, we present results for several experiments with comparisons to other methods.

5.1. Plug & play vs. one-time denoising

Since we train our denoiser to establish a mapping function between PBR and its residual towards the ground truth, the first experiment we investigated is how to use this denoiser. We compare two frameworks, *i.e.*, the plug & play framework [44] and the one-time denoising framework. The plug & play framework decouples the forward physical model and the denoising prior using the ADMM technique [10]. For one time denoising, we apply the residual denoiser once after the PBR has converged. One time denoising is considered because it is considerably faster than plug & play. From a computation point of view, one epoch of our PBR has comparable computation time to one layer of a fully-connected CNN. However, our residual denoiser has 17 layers, which requires more computation time for the plug & play method. While we generally expect plug & play to perform better, our experimental results show that, empirically, plug & play performs similarly to one-time denoising. We reason that this is related to our denoiser training process and the initialization of the high-res tensor. Our physical model, Fig. 6, involves a temporal transition process from an existing frame to a future frame. We initialize the high-res tensor with the reference intensity frame. In each PBR epoch, the reconstruction process produces artifacts that are similar to the degradations in the initialized image. However, our denoiser is trained to "recognize" this "degradation" and remove these artifacts. Therefore, our denoiser is most useful and efficient when applied after the PBR has converged. A comparison can be seen in Fig. 7.

5.2. Comparison with other denoisers

Since we decouple the problem as a PBR process and a denoising process, it is interesting to see whether a general denoiser can complete this task. We select several video clips from the testing classes and compare our results with two other denoisers, DnCNN [48] and FFDNet [49]. DnCNN is an end-to-end trainable deep CNN for image denoising with different Gaussian noise levels, *e.g.*, [0, 55]. During our testing of DnCNN we found that the pre-trained weights do not perform well. We retrained the network using the Need for Speed dataset with Gaussian noise. The FFDNet is a later variant of DnCNN with the inclusion of

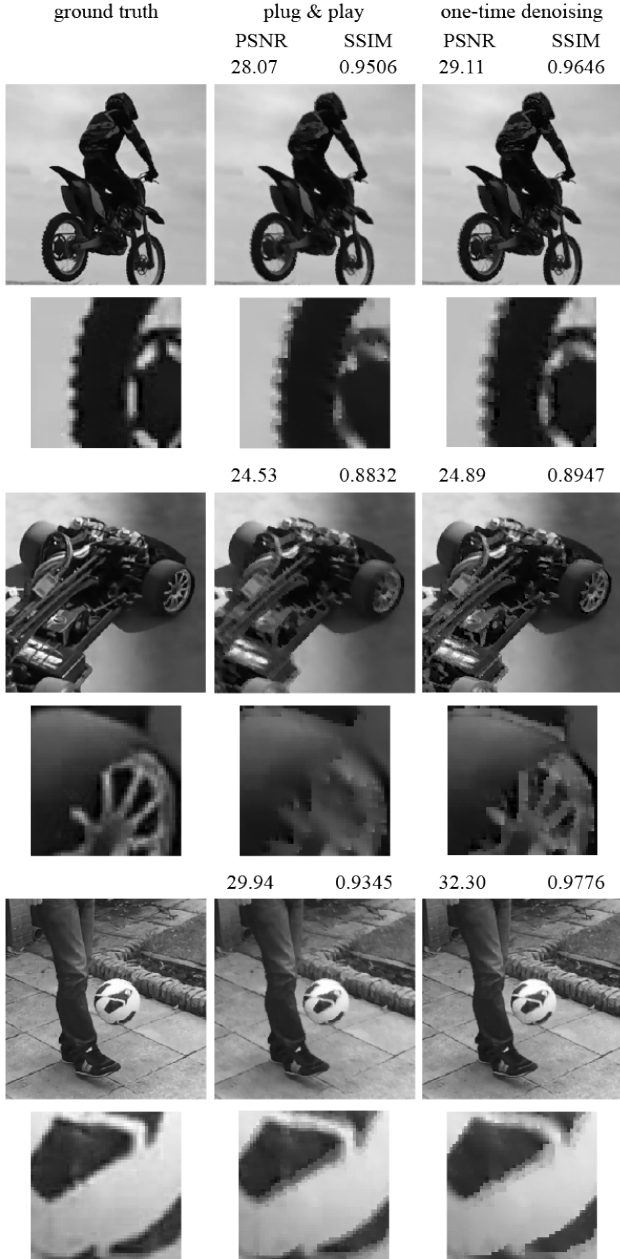


Figure 7: Plug & play vs. one-time denoising using our residual denoiser.

pre- and post-processing. During our tuning of the FFDNet, we found that smaller noise levels (a tunable parameter for using the model) result in better denoising performance in terms of PSNR and SSIM metrics. For each testing image, we present the best tuned FFDNet result (noise level less than 10) and compare with our proposed denoiser. The results are summarized in Table 2. A visualization of the results with zoom-in figures is presented in Fig. 8.

clip name	metric	PBR	DnCNN	FFDNet	Ours
airplane	PSNR	30.91	31.10	30.92	31.38
	SSIM	0.975	0.982	0.976	0.982
basketball	PSNR	23.55	24.05	23.47	24.06
	SSIM	0.963	0.971	0.964	0.972
soccer	PSNR	29.96	31.08	30.13	31.29
	SSIM	0.961	0.974	0.962	0.975
billiard	PSNR	36.46	35.42	36.48	36.46
	SSIM	0.982	0.986	0.983	0.987
ping pong	PSNR	32.46	32.26	32.50	32.24
	SSIM	0.974	0.978	0.975	0.979

Table 2: Performance comparison for different denoisers.

5.3. Frame interpolation

We compared our results for performing frame interpolation with a state-of-the-art approach, SepConv [34]. We present results comparing 3-frame interpolation in Fig. 9. We convert our grayscale testing images to 3 channels (RGB) before applying the SepConv interpolation algorithm. Although the results from SepConv provide better visual experience, they have salient artifacts around large motion regions. Note that performing intensity only frame interpolation produces significant artifacts in the presence of severe occlusions. On the other hand, our event-driven frame interpolation is able to successfully recover image details in occluded regions of interpolated frames. **Please see videos of results in supplementary material.** For a quantitative comparison, the SepConv method has an average SSIM of 0.9566 and PSNR of 29.79. Ours have average SSIM of 0.9741 and PSNR of 37.64.

5.4. Application to DAVIS dataset

We further apply our framework to the event camera dataset [32], which has captured intensity frames and event streams with corresponding timestamps. Our results involve two different forward models. The first one is frame interpolation, where our intensity operator can be expressed as $\mathcal{F}_i = \mathcal{H}_{10*i}, i \in \{0, 1\}$. For two video frames, we interpolate 9 frames in between. The events are binned evenly into 9 event frames. The results can be seen in Fig. 10. **More results and the converted videos can be found in the supplementary material.** The second forward model we used is a one-to-multiple frame motion deblurring model, *i.e.*, $\mathcal{F}_0 = \frac{1}{6} * \sum_{s=0}^5 \mathcal{H}_s$. In this case, we assume the observed intensity frame is an average of 6 frames. In Figure 10, row 2, we present the first and the last frame in our reconstruction. The motion of the shapes has been revealed. The corresponding video file can be seen in the supplementary material.

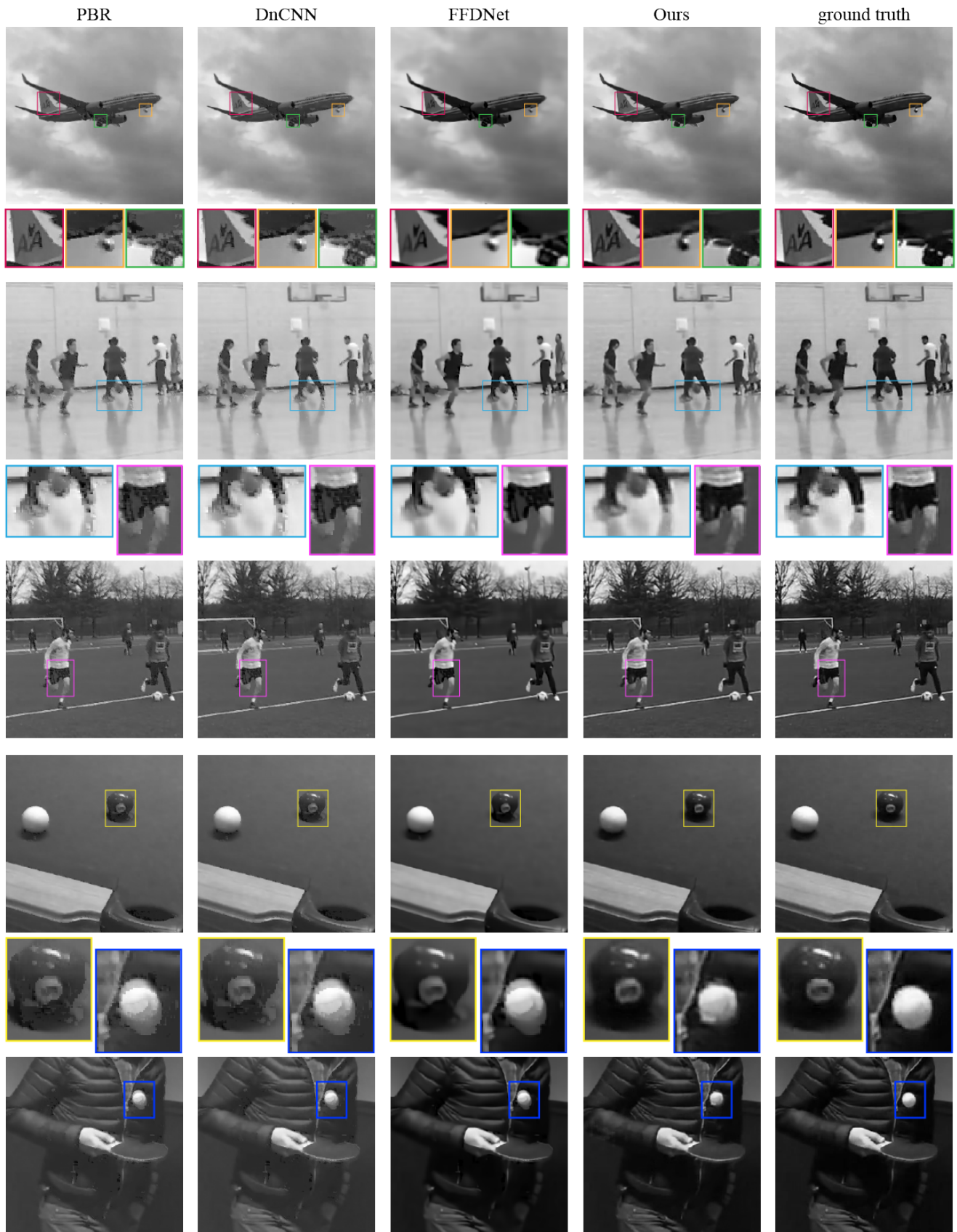


Figure 8: Performance comparison with other denoisers. Note that our method (second column from left) reconstructs interpolated frames with fewer motion artifacts. Superior reconstruction performance is clearly visible for the ping-pong ball in the bottom row (right inset), and the jet engine in the top row (middle inset).

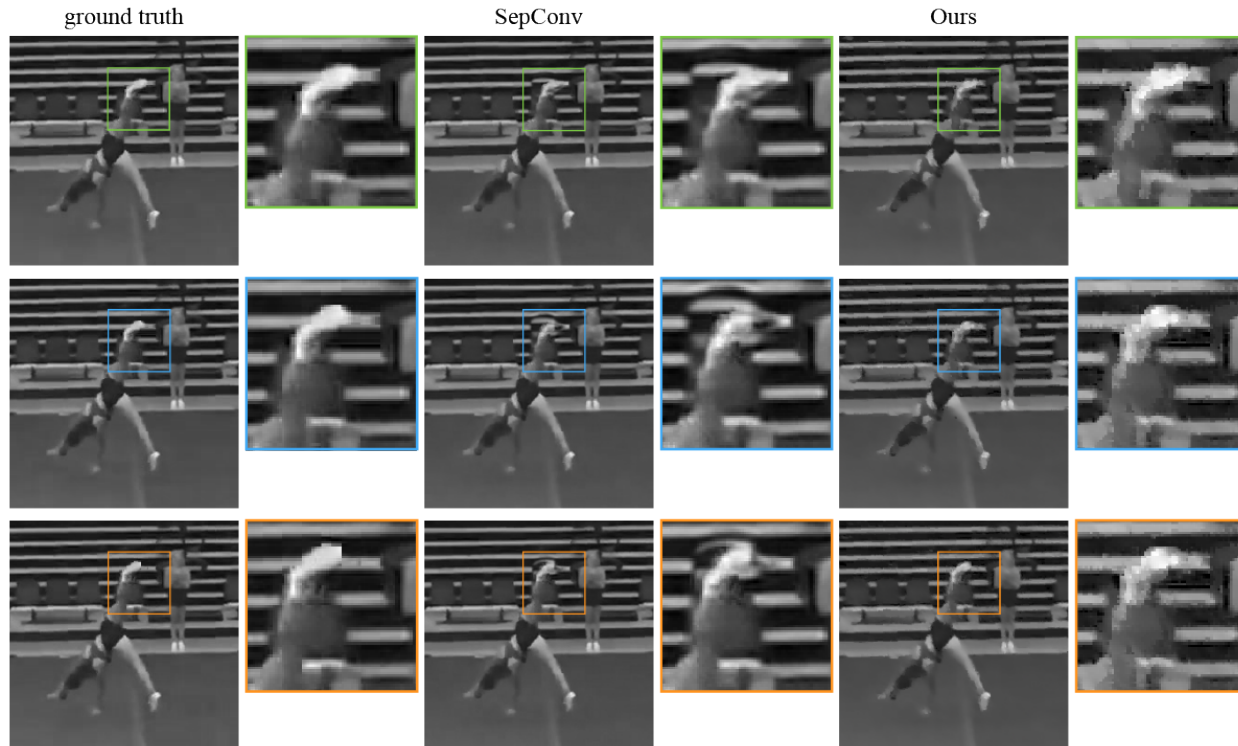


Figure 9: Multi-frame interpolation results, compared with SepConv [34]. The ground truth frames (first and last) are omitted, and only frames 2, 3 and 4 are shown from top to bottom. Note that the intensity-only based frame interpolation method (SepConv) produces considerable motion artifacts around occluded areas, while our event-driven frame interpolation successfully recovers image details in occluded regions. More results are shown in the supplementary material.

6. Conclusion

In this paper, we have demonstrated a novel framework for fusing intensity video frames with event streams. Our proposed framework involves a differentiable physical model to approximate the image formation process and a CNN based denoiser for further enhancement of the physically based reconstruction (PBR). Our experiments have shown that training a residual denoiser coupled with the PBR process can effectively fuse information from intensity frames and an event stream to recover high speed video. We demonstrated that our PBR process can effectively synthesize video frames in either frame interpolation or motion deblurring scenarios.

References

- [1] J. Ascenso, C. Brites, and F. Pereira. Improving frame interpolation with spatial motion smoothing for pixel domain distributed video coding. In *5th EURASIP Conference on Speech and Image Processing, Multimedia Communications and Services*, pages 1–6. Citeseer, 2005.
- [2] R. G. Baraniuk, T. Goldstein, A. C. Sankaranarayanan, C. Studer, A. Veeraraghavan, and M. B. Wakin. Compressive video sensing: algorithms, architectures, and applications. *IEEE Signal Processing Magazine*, 34(1):52–66, 2017.
- [3] P. Bardow, A. J. Davison, and S. Leutenegger. Simultaneous optical flow and intensity estimation from an event camera. In *Proceedings of the IEEE Conference on Computer Vision and Pattern Recognition*, pages 884–892, 2016.
- [4] S. Barua, Y. Miyatani, and A. Veeraraghavan. Direct face detection and video reconstruction from event cameras. In *Applications of Computer Vision (WACV), 2016 IEEE Winter Conference on*, pages 1–9. IEEE, 2016.
- [5] R. Benosman, C. Clercq, X. Lagorce, S.-H. Ieng, and C. Bartolozzi. Event-based visual flow. *IEEE transactions on neural networks and learning systems*, 25(2):407–417, 2014.
- [6] J. R. Bergen, P. Anandan, K. J. Hanna, and R. Hingorani. Hierarchical model-based motion estimation. In *European conference on computer vision*, pages 237–252. Springer, 1992.
- [7] R. Berner, C. Brandli, M. Yang, S.-C. Liu, and T. Delbruck. A 240×180 10mw 12us latency sparse-output vision sensor for mobile applications. In *VLSI Circuits (VLSIC), 2013 Symposium on*, pages C186–C187. IEEE, 2013.
- [8] P. Bhat, C. L. Zitnick, N. Snavely, A. Agarwala, M. Agrawala, M. Cohen, B. Curless, and S. B. Kang. Using photographs to enhance videos of a static scene. In *Proceedings of the 18th Eurographics conference on Rendering Techniques*, pages 327–338. Eurographics Association, 2007.

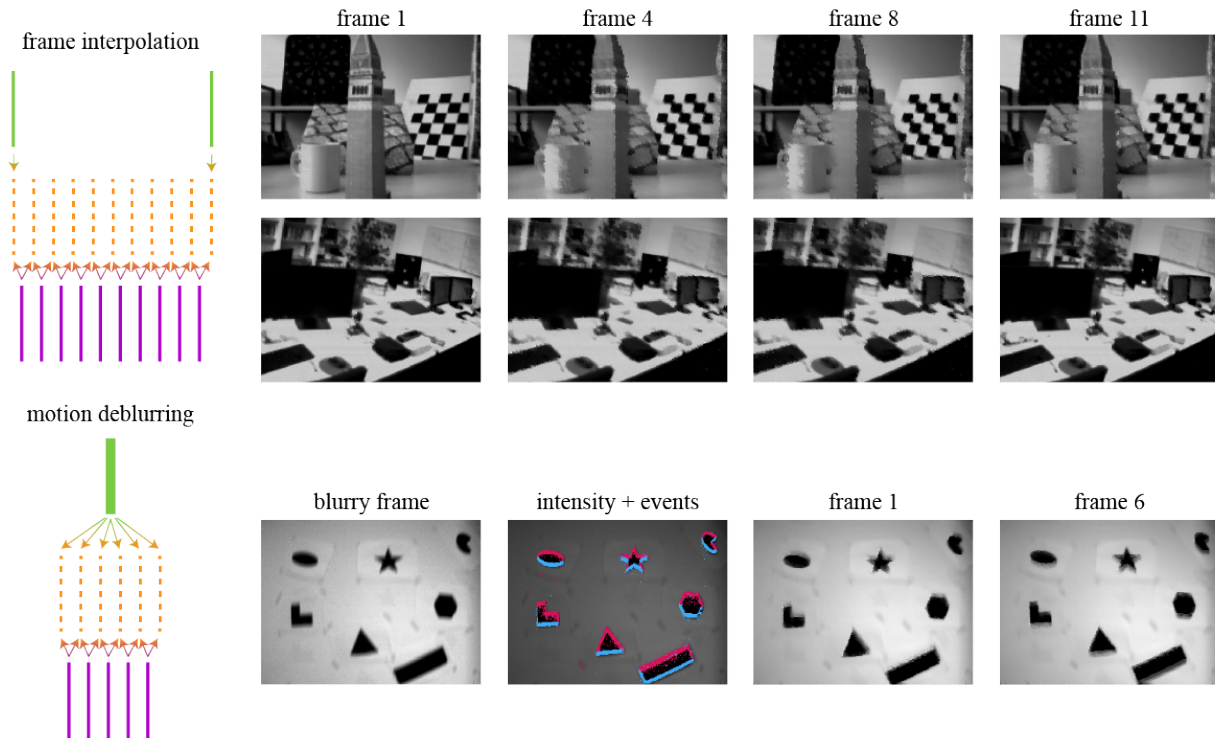


Figure 10: Applying our framework to the event camera dataset. We present results of two cases: multi-frame interpolation and image motion deblurring (from a single blurry image to a multi-frame video). The corresponding videos can be checked in our supplementary material.

- [9] P. Bhattacharjee and S. Das. Temporal coherency based criteria for predicting video frames using deep multi-stage generative adversarial networks. In *Advances in Neural Information Processing Systems*, pages 4271–4280, 2017.
- [10] S. Boyd, N. Parikh, E. Chu, B. Peleato, J. Eckstein, et al. Distributed optimization and statistical learning via the alternating direction method of multipliers. *Foundations and Trends® in Machine Learning*, 3(1):1–122, 2011.
- [11] T. Brosch, S. Tschechne, and H. Neumann. On event-based optical flow detection. *Frontiers in neuroscience*, 9:137, 2015.
- [12] B.-D. Choi, J.-W. Han, C.-S. Kim, and S.-J. Ko. Motion-compensated frame interpolation using bilateral motion estimation and adaptive overlapped block motion compensation. *IEEE Transactions on Circuits and Systems for Video Technology*, 17(4):407–416, 2007.
- [13] M. Cook, L. Gugelmann, F. Jug, C. Krautz, and A. Steger. Interacting maps for fast visual interpretation. In *Neural Networks (IJCNN), The 2011 International Joint Conference on*, pages 770–776. IEEE, 2011.
- [14] H. K. Galoogahi, A. Fagg, C. Huang, D. Ramanan, and S. Lucey. Need for speed: A benchmark for higher frame rate object tracking. In *Computer Vision (ICCV), 2017 IEEE International Conference on*, pages 1134–1143. IEEE, 2017.
- [15] A. Gupta, P. Bhat, M. Dontcheva, O. Deussen, B. Curless, and M. Cohen. Enhancing and experiencing spacetime resolution with videos and stills. In *Computational Photography (ICCP), 2009 IEEE International Conference on*, pages 1–9. IEEE, 2009.
- [16] M. Gupta, A. Agrawal, A. Veeraraghavan, and S. G. Narasimhan. Flexible voxels for motion-aware videography. In *European Conference on Computer Vision*, pages 100–114. Springer, 2010.
- [17] K. He, X. Zhang, S. Ren, and J. Sun. Deep residual learning for image recognition. In *Proceedings of the IEEE conference on computer vision and pattern recognition*, pages 770–778, 2016.
- [18] B. K. Horn and B. G. Schunck. Determining optical flow. *Artificial intelligence*, 17(1-3):185–203, 1981.
- [19] Z. Hu, Y. Ma, and L. Ma. Multi-scale video frame-synthesis network with transitive consistency loss. *arXiv preprint arXiv:1712.02874*, 2017.
- [20] E. Ilg, N. Mayer, T. Saikia, M. Keuper, A. Dosovitskiy, and T. Brox. FlowNet 2.0: Evolution of optical flow estimation with deep networks. In *IEEE Conference on Computer Vision and Pattern Recognition (CVPR)*, volume 2, 2017.
- [21] M. Iliadis, L. Spinoulas, and A. K. Katsaggelos. Deep fully-connected networks for video compressive sensing. *Digital Signal Processing*, 72:9–18, 2018.
- [22] H. Kim, A. Handa, R. Benosman, S.-H. Ieng, and A. J. Davison. Simultaneous mosaicing and tracking with an event camera. *J. Solid State Circ*, 43:566–576, 2008.

- [23] R. Krishnamurthy, J. W. Woods, and P. Moulin. Frame interpolation and bidirectional prediction of video using compactly encoded optical-flow fields and label fields. *IEEE transactions on circuits and systems for video technology*, 9(5):713–726, 1999.
- [24] P. Lichtsteiner, C. Posch, and T. Delbruck. A 128 x 128 120db 30mw asynchronous vision sensor that responds to relative intensity change. In *Solid-State Circuits Conference, 2006. ISSCC 2006. Digest of Technical Papers. IEEE International*, pages 2060–2069. IEEE, 2006.
- [25] Z. Liu, R. Yeh, X. Tang, Y. Liu, and A. Agarwala. Video frame synthesis using deep voxel flow. In *International Conference on Computer Vision (ICCV)*, volume 2, 2017.
- [26] P. Llull, X. Liao, X. Yuan, J. Yang, D. Kittle, L. Carin, G. Sapiro, and D. J. Brady. Coded aperture compressive temporal imaging. *Optics express*, 21(9):10526–10545, 2013.
- [27] B. D. Lucas, T. Kanade, et al. An iterative image registration technique with an application to stereo vision. 1981.
- [28] M. Luessi and A. K. Katsaggelos. Efficient motion compensated frame rate upconversion using multiple interpolations and median filtering. In *Image Processing (ICIP), 2009 16th IEEE International Conference on*, pages 373–376. IEEE, 2009.
- [29] A. I. Maqueda, A. Loquercio, G. Gallego, N. Garcia, and D. Scaramuzza. Event-based vision meets deep learning on steering prediction for self-driving cars. In *Proceedings of the IEEE Conference on Computer Vision and Pattern Recognition*, pages 5419–5427, 2018.
- [30] N. Matsuda, O. Cossairt, and M. Gupta. Mc3d: Motion contrast 3d scanning. In *2015 IEEE International Conference on Computational Photography (ICCP)*, pages 1–10. IEEE, 2015.
- [31] E. Mueggler, C. Bartolozzi, and D. Scaramuzza. Fast event-based corner detection. In *28th British Machine Vision Conference (BMVC)*, 2017.
- [32] E. Mueggler, H. Rebecq, G. Gallego, T. Delbruck, and D. Scaramuzza. The event-camera dataset and simulator: Event-based data for pose estimation, visual odometry, and slam. *The International Journal of Robotics Research*, 36(2):142–149, 2017.
- [33] G. Munda, C. Reinbacher, and T. Pock. Real-time intensity-image reconstruction for event cameras using manifold regularisation. *International Journal of Computer Vision*, 126(12):1381–1393, 2018.
- [34] S. Niklaus, L. Mai, and F. Liu. Video frame interpolation via adaptive convolution. In *CVPR*, volume 2, page 6, 2017.
- [35] H. Rebecq, G. Gallego, E. Mueggler, and D. Scaramuzza. Emvs: Event-based multi-view stereo3d reconstruction with an event camera in real-time. *International Journal of Computer Vision*, pages 1–21, 2017.
- [36] H. Rebecq, T. Horstschaefer, G. Gallego, and D. Scaramuzza. Evo: A geometric approach to event-based 6-dof parallel tracking and mapping in real time. *IEEE Robotics and Automation Letters*, 2(2):593–600, 2017.
- [37] D. Reddy, A. Veeraraghavan, and R. Chellappa. P2c2: Programmable pixel compressive camera for high speed imaging. In *Computer Vision and Pattern Recognition (CVPR), 2011 IEEE Conference on*, pages 329–336. IEEE, 2011.
- [38] B. Rueckauer and T. Delbruck. Evaluation of event-based algorithms for optical flow with ground-truth from inertial measurement sensor. *Frontiers in neuroscience*, 10:176, 2016.
- [39] P. Sand and S. Teller. Particle video: Long-range motion estimation using point trajectories. *International Journal of Computer Vision*, 80(1):72, 2008.
- [40] F. Schubert and K. Mikolajczyk. Combining high-resolution images with low-quality videos. In *BMVC*, pages 1–10, 2008.
- [41] E. Shechtman, Y. Caspi, and M. Irani. Space-time super-resolution. *IEEE Transactions on Pattern Analysis and Machine Intelligence*, 27(4):531–545, 2005.
- [42] V. Stanković, L. Stanković, and S. Cheng. Compressive video sampling. In *Signal Processing Conference, 2008 16th European*, pages 1–5. IEEE, 2008.
- [43] J. Tarvainen, M. Nuutinen, and P. Oittinen. Spatial and temporal information as camera parameters for super-resolution video. In *Multimedia (ISM), 2012 IEEE International Symposium on*, pages 302–305. IEEE, 2012.
- [44] S. V. Venkatakrisnan, C. A. Bouman, and B. Wohlberg. Plug-and-play priors for model based reconstruction. In *Global Conference on Signal and Information Processing (GlobalSIP), 2013 IEEE*, pages 945–948. IEEE, 2013.
- [45] Z. Wang, L. Spinoulas, K. He, L. Tian, O. Cossairt, A. K. Katsaggelos, and H. Chen. Compressive holographic video. *Optics express*, 25(1):250–262, 2017.
- [46] A. Wedel, T. Pock, J. Braun, U. Franke, and D. Cremers. Duality tv-l1 flow with fundamental matrix prior. In *Image and Vision Computing New Zealand, 2008. IVCNZ 2008. 23rd International Conference*, pages 1–6. IEEE, 2008.
- [47] H. Zabrodsky and S. Peleg. Attentive transmission. *Journal of Visual Communication and Image Representation*, 1(2):189–198, 1990.
- [48] K. Zhang, W. Zuo, Y. Chen, D. Meng, and L. Zhang. Beyond a gaussian denoiser: Residual learning of deep cnn for image denoising. *IEEE Transactions on Image Processing*, 26(7):3142–3155, 2017.
- [49] K. Zhang, W. Zuo, and L. Zhang. Ffdnet: Toward a fast and flexible solution for cnn based image denoising. *IEEE Transactions on Image Processing*, 2018.